



Article

Dissimilar Laser Welding of a NiTi Shape Memory Alloy to Ti₂AlNb

Fuguo Ge ¹, Bei Peng ¹, João Pedro Oliveira ² , Wenchao Ke ¹ , Fissaha Biruke Teshome ¹ , Yongmei Li ³ and Zhi Zeng ^{1,*}

¹ School of Mechanical and Electrical Engineering, University of Electronic Science and Technology of China, Chengdu 611731, China; gfg18200141721@163.com (F.G.); beipeng@uestc.edu.cn (B.P.); ke@std.uestc.edu.cn (W.K.); fishbiruke@gmail.com (F.B.T.)

² UNIDEMI, Department of Mechanical and Industrial Engineering, NOVA School of Science and Technology, NOVA University Lisbon, 2829-516 Caparica, Portugal; jp.oliveira@fct.unl.pt

³ Beijing North Vehicle Group Corporation, Beijing 100072, China; kiwilily@163.com

* Correspondence: zhizeng@uestc.edu.cn; Tel.: +86-028-61830229

Abstract: NiTi-based shape memory alloys and the Ti₂AlNb alloy have gained increasing importance in the aerospace field. The joining of these two materials can further increment the importance and usage of these relevant engineering materials and expand their potential applications. However, when joining NiTi-based shape memory alloys to Ti-based alloys, the formation of brittle Ti-rich intermetallic compounds often occurs, significantly limiting their functionality and use. Dissimilar joints between a NiTi shape memory alloy and Ti₂AlNb alloy were obtained using a 0.1 mm thick Niobium (Nb) interlayer via laser welding. By process optimization, sound joints were obtained. The microstructure evolution was assessed by means of electron microscopy, whereas the mechanical strength of the joints was evaluated using lap shear tensile testing. The best performing joints were seen to fracture at maximum loads above 1230 N, thus allowing us to consider this dissimilar pair for structural applications.

Keywords: NiTi shape memory alloys; Ti₂AlNb; Nb interlayer; laser welding; microstructure; mechanical properties



Citation: Ge, F.; Peng, B.; Oliveira, J.P.; Ke, W.; Teshome, F.B.; Li, Y.; Zeng, Z. Dissimilar Laser Welding of a NiTi Shape Memory Alloy to Ti₂AlNb. *Metals* **2021**, *11*, 1578. <https://doi.org/10.3390/met11101578>

Academic Editor: Aleksander Lisiecki

Received: 11 September 2021

Accepted: 30 September 2021

Published: 4 October 2021

Publisher's Note: MDPI stays neutral with regard to jurisdictional claims in published maps and institutional affiliations.



Copyright: © 2021 by the authors. Licensee MDPI, Basel, Switzerland. This article is an open access article distributed under the terms and conditions of the Creative Commons Attribution (CC BY) license (<https://creativecommons.org/licenses/by/4.0/>).

1. Introduction

Due to their unique properties of superelasticity (SE) and shape memory effect (SME), NiTi shape memory alloys are involved in a wide range of applications, including aerospace, biomedicine, energy development, and machinery, as well as other fields [1–3]. The joining of NiTi to itself or to other materials is therefore inevitable, as together these alloys possess extraordinary functions. Ti₃Al-based alloys and Ti₂AlNb alloys have various advantages, including possessing low density, high specific strength, good oxidation resistance, as well as excellent creep resistance and fatigue resistance. Ti₂AlNb is one of the most promising lightweight, high-temperature structural materials for aerospace applications [4,5]. It can be used in a temperature range of 650 to 750 °C [6,7], which can have a significant impact in reducing an aircraft's weight, improving fuel efficiency and high-temperature service performance [8]. Therefore, it is of great significance to connect these two advanced engineering materials and expand their functional/structural applications.

There are many works on the methods of connecting Ti-Al alloys in similar combinations, including friction welding [9,10], electron beam welding [11,12], diffusion welding [13,14], brazing [15] and wire and arc additive manufacturing [16]. Scholarly work on dissimilar connections were primarily focused on titanium and steel connections [17,18]. The progress of this research in creating autogenous and dissimilar welds for NiTi shape memory alloy in various joint configurations has been reported in the literature [19–21]. Due to the significant difference in the composition between Ti-Al alloys and Ni-based

alloys, the physical and chemical properties of these alloys can also be significantly varied, leading to severe problems in direct connection [22–24]. Peng et al., [25] laser welded a NiTi alloy to Ti6Al4V and found the presence of brittle NiTi₂ intermetallic compounds, which can promote a decrease in the joint strength and ductility. Shiue and Wu [26] found that NiTi and Ti6Al4V alloys can be successfully joined using a 50 µm thickness BAg-8 interlayer by infrared brazing technology. However, the tensile strength of the joint was only 200 MPa. Ti and Ni can easily form NiTi₂ and Ni₃Ti intermetallic compounds due to their strong affinity and the occurrence of chemical reactions within the melt pool. These brittle phases can seriously deteriorate the mechanical properties of the joint.

Laser welding has been widely used as an effective joining method for creating dissimilar joints as it possesses key advantages such as high energy density, reduced extension of the thermally affected regions, and low residual stresses [27,28]. Although research on the laser weldability of Ti₃Al-based alloys has gained special interest after the 1990s, few studies have focused on the use of a laser source to weld Ti₂AlNb alloys. Currently, there is a lack of systematic and in-depth research on the relationship between process parameters, microstructure evolution, and joint performance when it comes to dissimilar welding of Ti₂AlNb to NiTi-based alloys. We bridge this gap in this work by joining for the first time a NiTi shape memory alloy to the Ti₂AlNb alloy. To reduce and/or avoid the formation of brittle intermetallic compounds, a solid interlayer is used between both base materials. An interlayer with a melting point higher than the two different base materials has proved to be a successful barrier to diffusion and mixing, thus improving the joint performance [29–31].

In this work, laser-welded NiTi-Ti₂AlNb dissimilar joints were obtained using a Nb interlayer. The microstructure, mechanical properties and fracture mechanism of the joints were studied in this paper. This work is of great significance for applying complex components composed of dissimilar joints made of Ti₂AlNb and NiTi.

2. Materials and Methods

NiTi (51.9 at% Ni) shape memory alloy sheets with the dimension of 100 mm × 10 mm × 0.7 mm (length × width × thickness) and Ti₂AlNb (87.6 at% Ti) sheets with the dimension of 100 mm × 10 mm × 0.6 mm were used in the laser welding experiments. Nb (99.9% purity) foils with 30 mm × 10 mm × 0.1 mm size were chosen as the interlayer material.

Before welding, a fine sandpaper was used to polish and remove the oxide film on the surface of each workpiece. Then, the specimens were cleaned with acetone and ethanol, and subsequently dried. A high power YAG laser W-LTA4030 (HGTECH, Wuhan, China), produced by HGTEC, with a wavelength of 1070 nm was used to create lap joints between NiTi and Ti₂AlNb alloys. Several experiments were performed to optimize the welding parameters. The ranges of welding power (*P*) and welding speed (*v*) were changed from 900 to 1300 W and 1.5 to 4.0 mm/s, respectively. The total length of the weld was 8 mm. In this investigation, the NiTi sheet was placed on the top of the Ti₂AlNb sheet, as detailed in Figure 1. The welding specimens were fixed using a special welding fixture, which was designed to minimize the gap between the base materials. Pure argon was used as the shielding gas at a flow rate of 20 L/min to prevent oxidation. The shielding gas was inserted both at the front and back of the weld.

The detailed experimental parameters for the laser welding experiments are depicted in Table 1.

The welded joints were cut into small metallographic specimens, mounted in epoxy resin, mechanically ground with sandpaper from 600 to 1500 grit, polished and etched for microstructure analysis. The microstructure of the samples was analysed using an Olympus BX53M optical microscope (OM, OLYMPUS, Tokyo, Japan). Furthermore, a scanning electron microscope (SEM, HITACHI, Tokyo, Japan), equipped with an Energy Dispersive X-ray (EDS) system was used to further assess the joint's microstructure features. An Instron 5548 micro-tensile tester (INSTRON, Boston, MA, USA) was used to measure

the tensile strength of dissimilar lap joints with a displacement speed of 1.5 mm/min at room temperature. Three samples were tested under each experimental parameter to determine the shear force. The microstructure of the fractured surfaces was observed on the SEM.

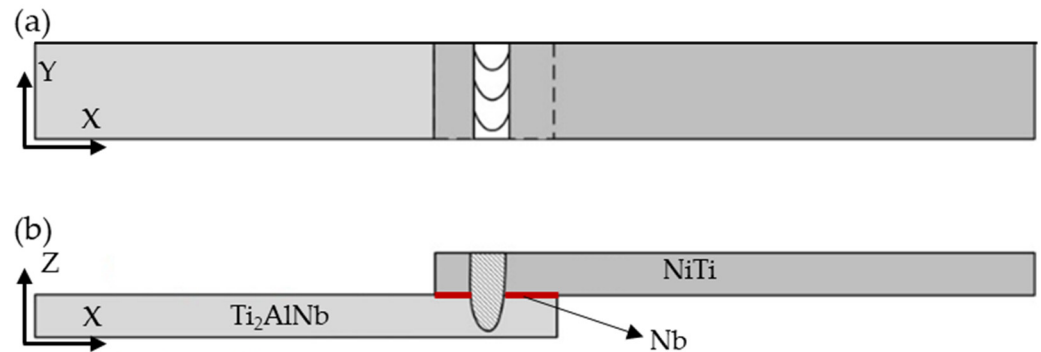


Figure 1. Schematic diagram of lap test: (a) Welded specimen in the X-Y plane; (b) Welded specimen in the X-Z plane.

Table 1. Laser welding parameters.

Experiment No.	Laser Power (W)	Welding Speed (mm/s)
1	900	3.0
2	1000	3.0
3	1100	3.0
4	1200	3.0
5	1300	3.0
6	1100	1.5
7	1100	2.0
8	1100	2.5
9	1100	3.5
10	1100	4.0

3. Results and Discussion

3.1. Macro Morphology and Microstructure of Welded Joint

Figure 2 depicts the bead's appearance on the front side of the joint made with a 1100 W laser power and 3 mm/s of welding speed (No. 3 sample). It could be seen that the surface of the weld had a bright, silver metallic luster aspect, indicating that the surface of the weld was not contaminated by oxygen or nitrogen. The appearance of the intermetallic compound NiTi₂ resulted in a brittle weld and caused cracks in the welded joint upon cooling due to thermal stresses that developed [25,32]. Hydrides in the weld could also cause the weld to fracture [10,33]. The weld surface of the lap joint was well-formed; no defects such as cracks and bead collapse were observed according to the macroscopic appearance of the joint.

Figure 3 details the macroscopic morphology of the cross-section of the welded joint when the laser power was 1100 W and the welding speed was 3 mm/s (No. 3 sample). It can be well observed that the fusion zone penetrates the Nb interlayer towards the Ti₂AlNb sheet along the Z-axis direction. The weld penetration depth at the Ti₂AlNb plate was close to 62 % of the thickness of the base metal, corresponding to roughly 370 μm. Compared to NiTi and Ti₂AlNb, Nb has a relatively high thermal conductivity (18.0 W m⁻¹ K⁻¹ and 7.4 W m⁻¹ K⁻¹ for NiTi and Ti₂AlNb, while for Nb the value is of 52.3 W m⁻¹ K⁻¹) [34–36] and can conduct the laser heat from the NiTi toward the Ti₂AlNb sheet. Nb can undergo a eutectic reaction with NiTi according to the pseudo-binary NiTi-Nb phase diagram, preventing the formation of brittle intermetallic compounds [34].

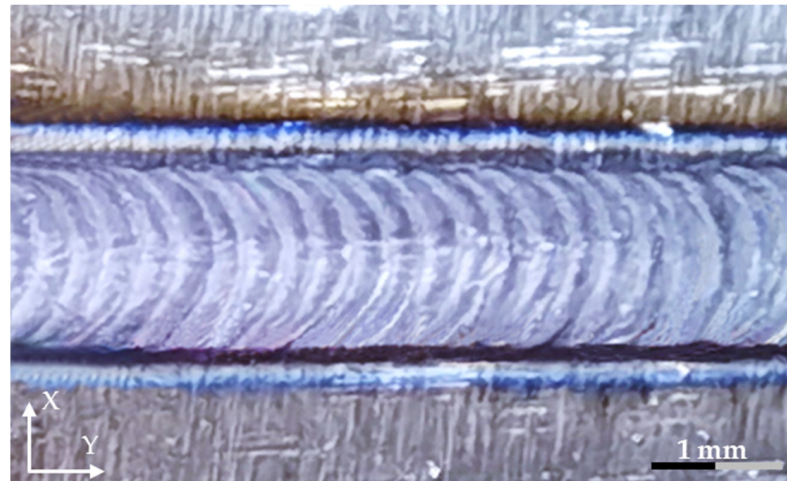


Figure 2. Overall macroscopic morphology of the weld joint (No. 3 sample).

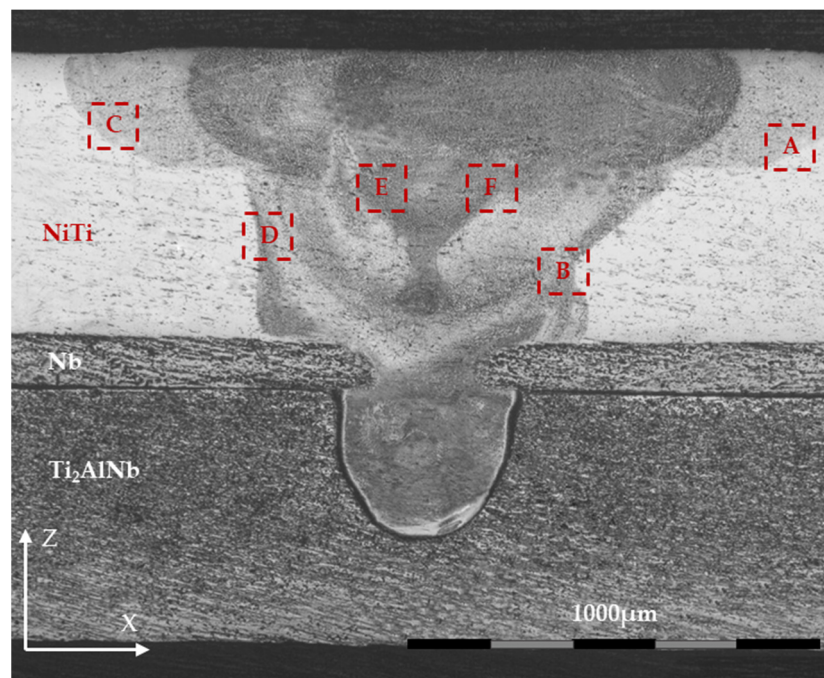


Figure 3. Macro morphology of weld cross section (No. 3 sample).

The weld width on the Ti_2AlNb sheet was smaller than that of the NiTi sheet, while it appeared to be larger than that of the Nb interlayer in the X-axis direction, which was caused by the gradual heat loss along the Z-axis. The maximum width on the top weld of the NiTi sheet was about 1830 μm and the maximum width of the Ti_2AlNb sheet was 430 μm , while the width of the Nb interlayer was 300 μm . The temperature gradient experienced by each material along the thickness of the weld was responsible for such a difference in width. The temperature on the top surface of the weld was higher than that on the bottom surface, which caused more material to melt. Nb is a refractory metal with a melting point of 2477 $^{\circ}C$, which is significantly higher than those of NiTi (1310 $^{\circ}C$) and Ti_2AlNb (1746 $^{\circ}C$) [37,38], resulting in a narrow melting width in the weld. Although Ti_2AlNb was positioned at the bottom of the joint, the heat was enough to partially melt its thickness. Melting of the Ti_2AlNb sheet was also assisted by the high thermal conductivity of Nb.

To evaluate the microstructures of the joint, high magnification photos obtained at different locations within the joint (spots A, B, C, D, E and F in Figure 3) on the NiTi side

are depicted in Figure 4. The dendrites nucleated from the cold base material and grew up towards the weld centreline. The low heat input of laser welding associated with the high cooling rates of the process promotes the formation of refined dendrites. Near-equiaxed grains were also observed in the central zone of the weld, as shown in Figure 4e,f, which corresponds to regions E and F of Figure 3. The high temperature in the centre of the weld and change in thermal gradient across the fusion zone was helpful in promoting the formation of such grains. Typically, the presence of equiaxed grains is preferable as it can improve joint strength and toughness.

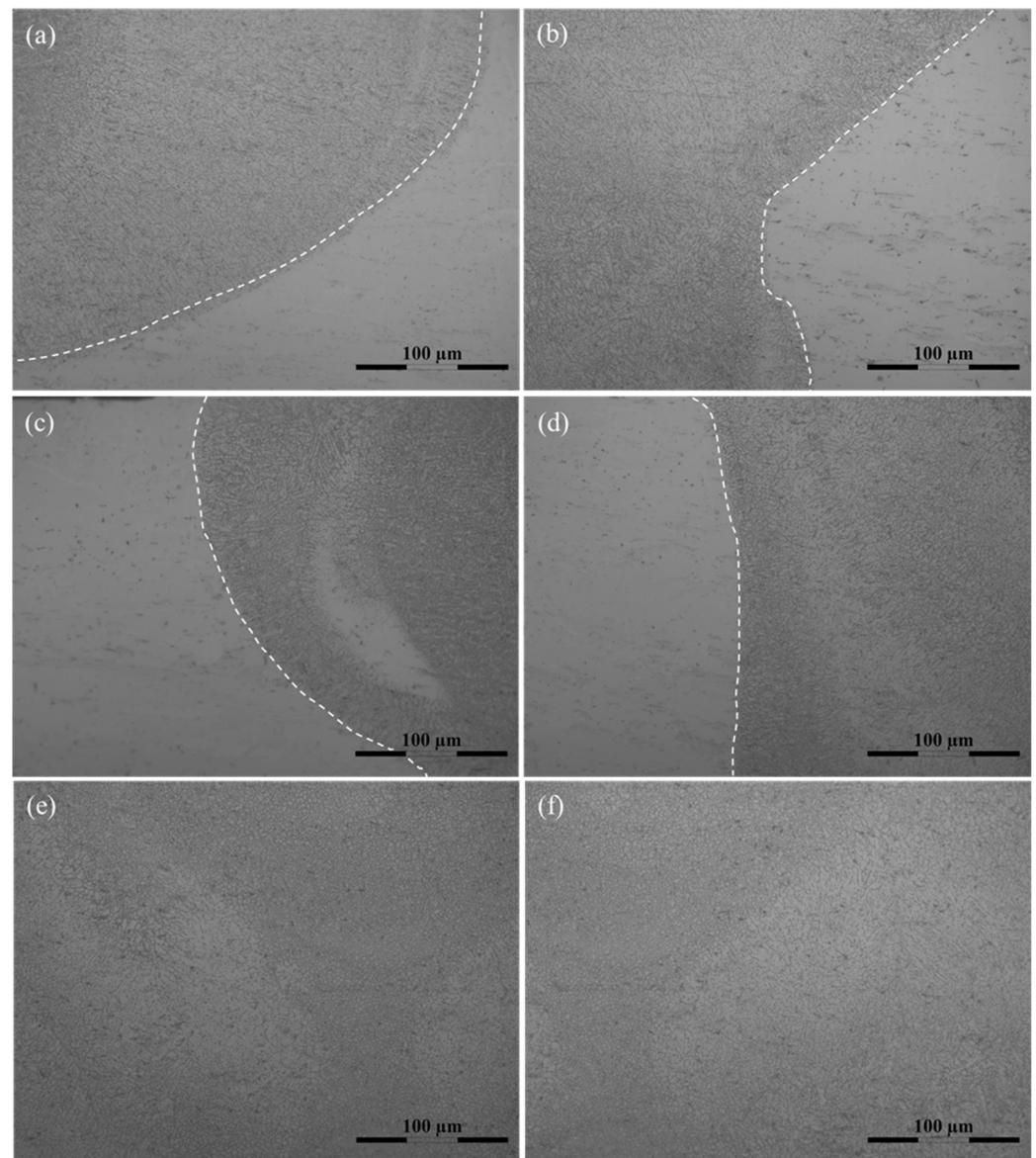


Figure 4. Microstructures of different zones on Figure 3 (No. 3 sample): (a) A zone; (b) B zone; (c) C zone; (d) D zone; (e) E zone; (f) F zone. (The white dotted line indicates the fusion zone boundary).

SEM images of the interfaces between the Nb and both the NiTi and the Ti_2AlNb base materials are shown in Figure 5a. The red circle was the starting point for the line scan. As shown in Figure 5b,c, the Nb interlayer formed defect-free interfaces with the NiTi sheet, while there was a small gap between Ti_2AlNb and the Nb interlayer at a particular distance from the centre of the weld, which might aid in fracture propagation upon mechanical testing.

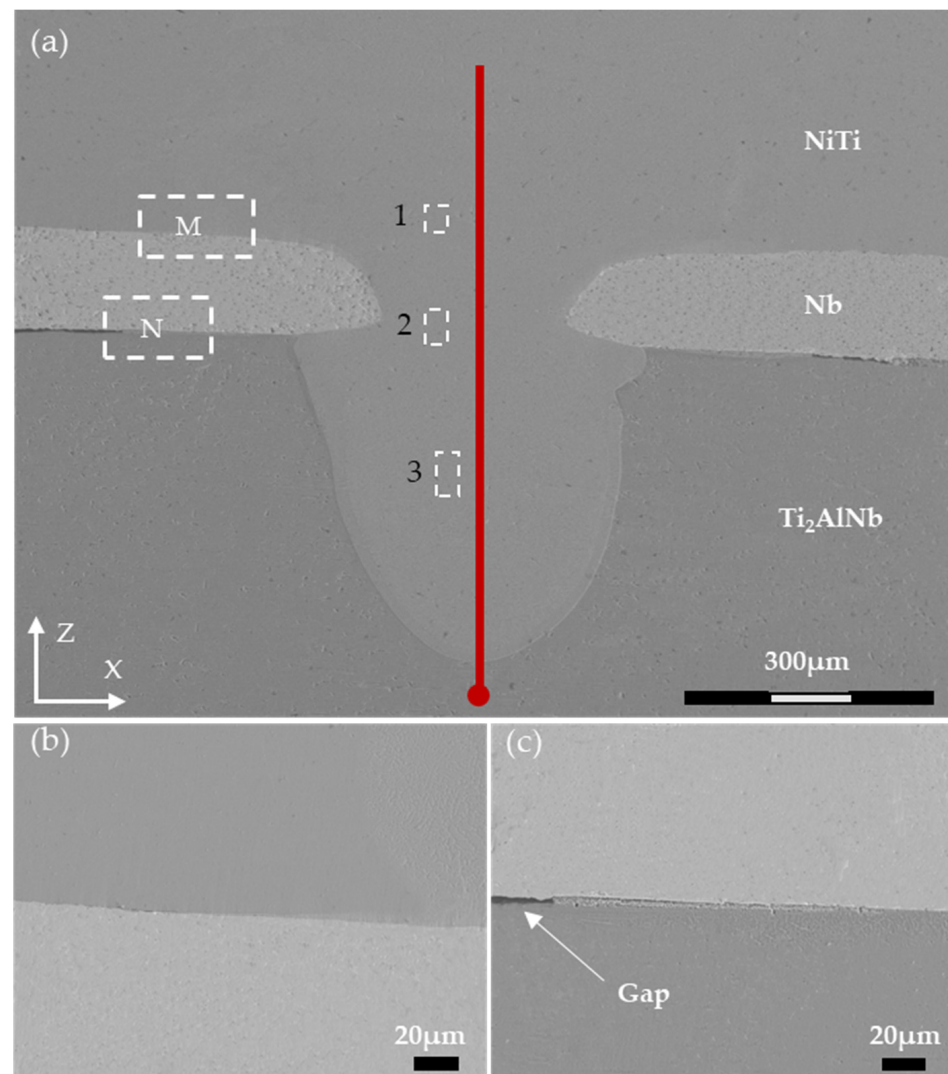


Figure 5. SEM images of: (a) Interface between NiTi, Nb and Ti₂AlNb; (b) Zone M of Figure 5a; (c) Zone N of Figure 5a. (The red line represents the EDS line analysis.) (No. 3 sample).

The line EDS analysis results are depicted in Figure 6. It can be observed that the intensity of Ni and Nb remains practically constant within the fusion zone. At some locations minor shifts in composition are observed, which can be attributed to the Marangoni effect resulting from the melting and mixing of the three materials. Another interesting point is the fact that Nb exists in both the NiTi and Ti₂AlNb regions. The Nb interlayer can constitute a protective barrier, which is beneficial to improve the performance of the welded joint [30,31]. Nb can exist in the form of solid solution in both alloys and, depending on the atomic percentage, it can promote the formation of new phases in both base materials [39,40]. Table 2 details the results of EDS chemical analysis in regions 1, 2 and 3 of Figure 5a. The atomic ratio of Ti and Ni in the three regions is close to 1, and the chemical constitutions were very close to original NiTi base material. In fact, up to 3 at. % of Nb can be dissolved in NiTi. As observed in the electron microscopy images, no secondary phases were seen, which further suggest that Nb-enriched NiTi solid solution was formed [41]. Previous work has shown that NiTi-Nb hypoeutectic structures can be formed when the Nb content ranges between 3 and 20 at. % [42].

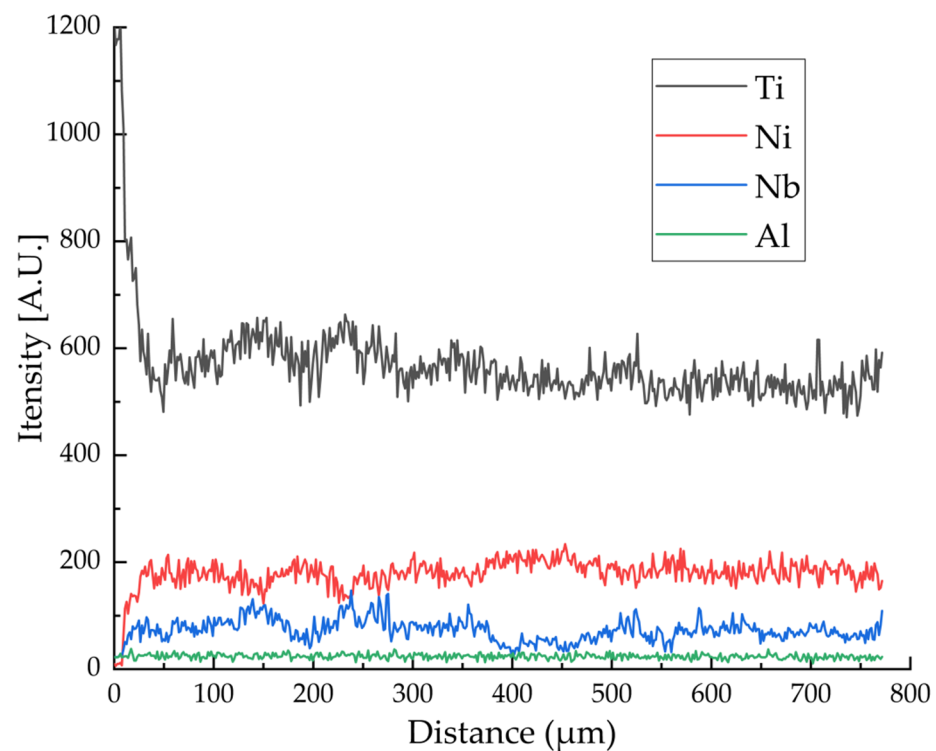


Figure 6. EDS line scans across the NiTi-Nb-Ti₂AlNb interface (No. 3 sample).

Table 2. Chemical analysis of different regions in Figure 5a (at. %, No. 3 sample).

Region	Ti	Ni	Nb
1	51.80	45.90	2.30
2	51.15	47.22	1.63
3	53.15	42.26	4.59

3.2. Mechanical Properties of Lap Joint Tensile

Keeping other factors constant, changes in the laser power (P) and welding speed (v) directly affect the energy input during welding. The laser power is positively correlated with heat input, but the welding speed is negatively correlated with heat input. Therefore, without considering efficiency, the relationship between the laser heat input (Q) and these welding parameters can be expressed as $Q = P/v$.

Figure 7 details a summary of the mechanical properties obtained after tensile lap shear testing joints obtained with different combinations of process parameters, keeping the welding speed constant at 3 mm/s. When the laser power was 900 W, the lap joint tensile strength was 967 N; when the laser power was 1100 W, the lap joint tensile strength was 1236 N, which was the highest tensile strength, and the corresponding maximum displacement was 1.26 mm; when the laser power was 1300 W, the lap joint tensile strength was 1069 N. Figure 7b shows the average tensile strength of lap joints under different laser powers. The tensile strength of the lap joints first increased and then decreased with the increase of laser power, which was caused by the continuous increment in heat input. resulting from the rise in power and constant speed. When the laser power was 900 W and 1000 W, the laser heat input was insufficient to promote a sound joint, resulting in lower strength. The heat conduction gradually reduced along the decreasing direction of the temperature gradient of the weld, resulting in a smaller cladding area on the Ti₂AlNb side and less molten metal. Although the NiTi sheet was well joined to the Nb interlayer, the connection strength between the Ti₂AlNb sheet and the Nb interlayer was weak. When the laser power was 1200 W and 1300 W, the larger laser heat input would cause a severe collapse of the weld surface, and even burn through the weld, thus reducing its strength.

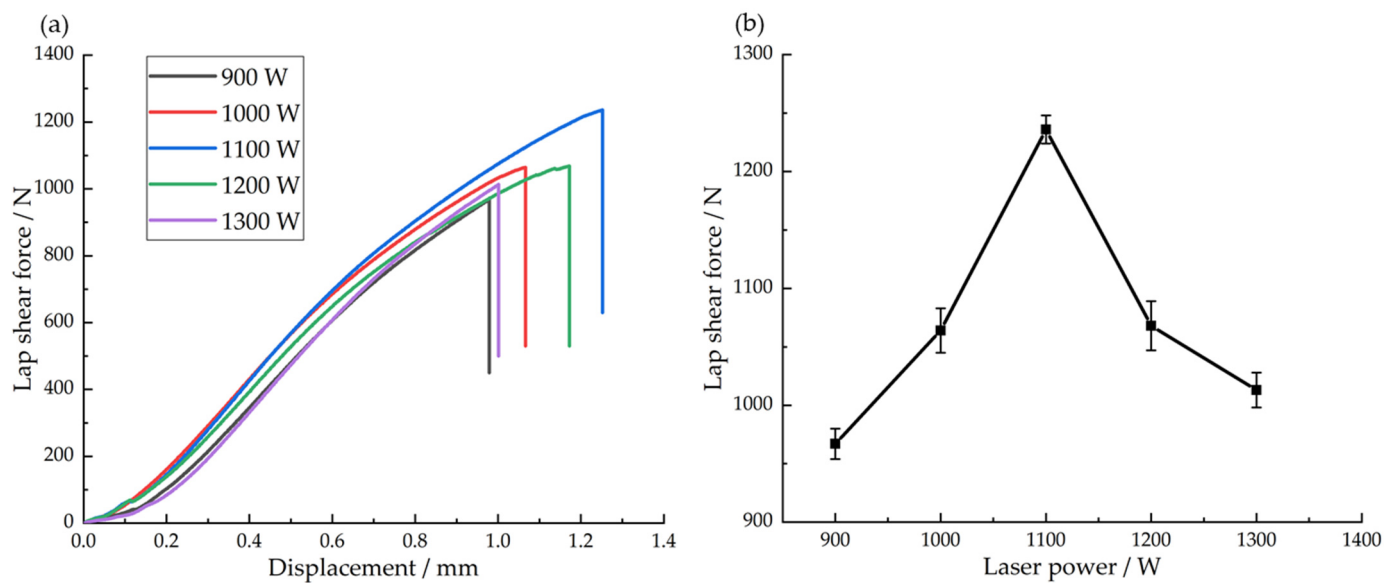


Figure 7. Effect of laser power on lap tensile shear force: (a) Representative lap tensile shear testing under different laser powers; (b) Mean value of lap tensile resistance under different laser powers.

Figure 8 shows the tensile strength of the lap joint when the laser power was kept constant at 1100 W, while the welding speed was varied. When the welding speed was 1.5 mm/s, the lap joint tensile strength was 1052 N; when the welding speed was 4 mm/s, the lap joint tensile strength was 1048 N, while the welding speed was 3 mm/s, the maximum tensile strength of 1236 N was obtained. Figure 8b details the average tensile strength of lap joints for different welding speeds. The tensile strength of the lap joints increased first and then decreased with the increase of welding speed. This is related to the variation in heat input of laser welding, which was continuously decreasing when the laser power was kept constant, while the welding speed was increased. Similarly, to what was previously explained when addressing the impact on changing the laser power, when the welding speed was too low, the heat input during welding was excessive, causing the weld to burn through the materials and reduce the tensile strength. When the welding speed was too high, insufficient heat was given to the materials making the weld depth too shallow, resulting in a decrease in the strength of the welded connection.

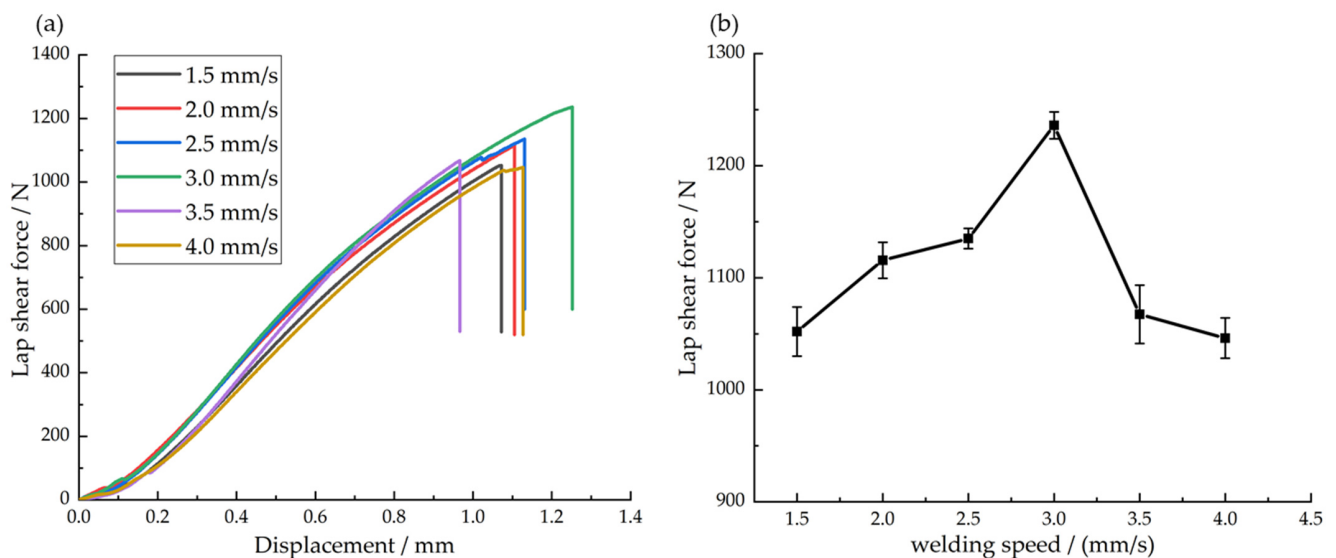


Figure 8. Effect of welding speed on lap tensile shear force: (a) Representative lap tensile shear testing under different welding speeds; (b) Mean value of lap tensile resistance under different welding speeds.

The tensile strength of dissimilar NiTi-Ti₂AlNb lap joint was ultimately determined by the welding parameters. When the heat input energy was too low, the materials could not be effectively joined. On the other hand, the weld would collapse when the heat input energy was very high. Therefore, proper control of the heat input is fundamental to improve the joint's mechanical properties.

3.3. Fracture Characteristics of Lap Joint

In this work, two fracture modes were observed by changing the laser power and welding speed. The broken positions of fracture mode I and fracture mode II occurred at the interface between Nb interlayer and Ti₂AlNb and the weld centre of the NiTi sheet, respectively. The tensile fracture specimens of experiments No. 3 and No. 5 were used to analyse the fracture mechanisms of the two fracture modes in this subsection.

When the laser power was 1100 W and the welding speed was 3 mm/s (condition No. 3), the NiTi sheet, Nb interlayer, and Ti₂AlNb sheet were effectively joined, which resulted in maximum tensile strength. As shown in Figure 9, the broken position occurred at the bottom of the joint on the Ti₂AlNb alloy side (defined as fracture mode I), while NiTi and Nb interlayer were firmly bonded together. The strength of the fusion zone dictated by the Nb interlayer and NiTi sheet mixing, which was higher than the fusion zone created by the Nb interlayer and Ti₂AlNb sheet. This can be related to the hypoeutectic bonding zone formed between Nb and NiTi [42]. The above EDS analysis (refer to Table 2) results indicated that a NiTi-Nb hypoeutectic structure existed in the weld area. The starting point of the fracture might be at the previously observed small gap existing between the Ti₂AlNb and Nb interlayer. When the laser power was 1300 W, and the welding speed was 3 mm/s (condition No. 5), the width and depth of the weld on the Ti₂AlNb side were further increased, and the fracture position was located on the centre of the NiTi side (defined as fracture mode II), as shown in Figure 10. Although the penetration depth of the weld was effectively increased, excessive heat input resulted in a burned weld and subsequent decrease in the strength of the joint.

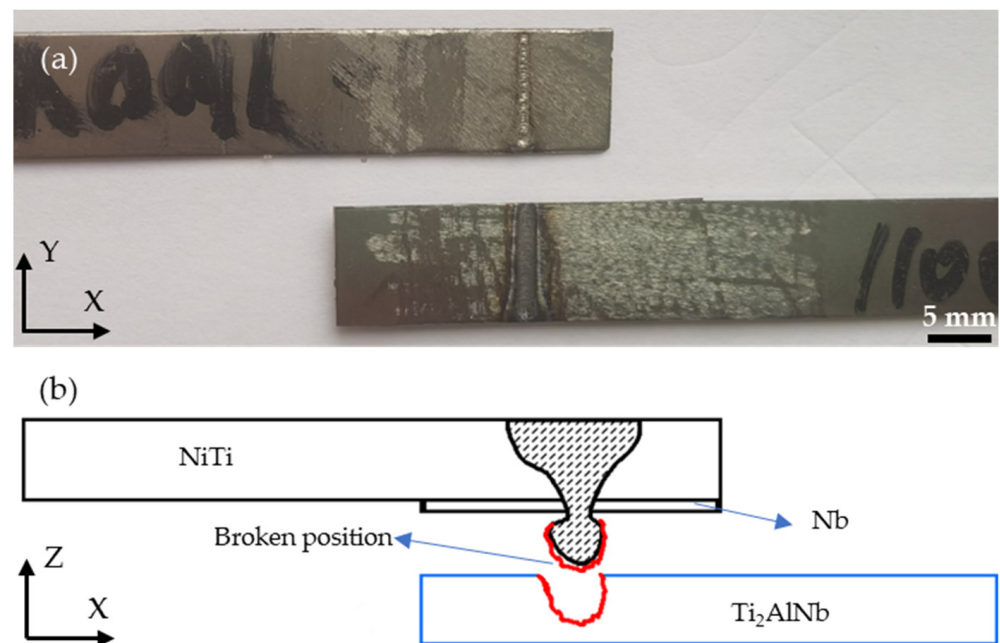


Figure 9. Fracture mode I: (a) Tensile fracture specimen; (b) Schematic diagram of fracture (The red line indicates the fracture surface).

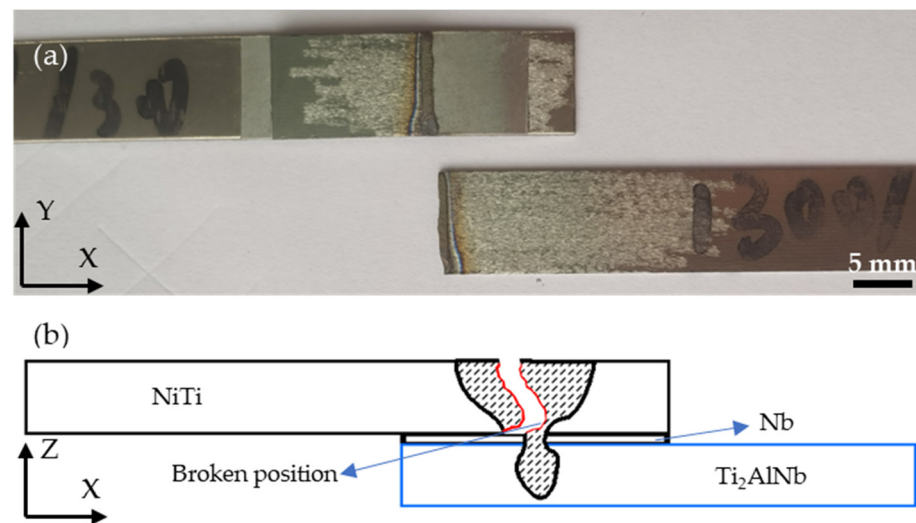


Figure 10. Fracture mode II: (a) Tensile fracture specimen; (b) Schematic diagram of fracture (The red line indicates the fracture surface).

The micrographs of the fracture interface under the two identified fracture modes are shown in Figures 11 and 12, respectively. Figure 11a illustrates an SEM image of the fractured joint on the Ti_2AlNb side. It can be observed that there are tearing characteristics along the weld interface. As shown in Figure 11b, marks with cleavage characteristics and some microcracks were found. The hydrogen and oxygen absorbed by the molten pool on the Ti_2AlNb side made the fracture surface brittle [33,43,44], which could have caused the weld strength to weaken. Micro pores were observed in Figure 12a, which might be due to the high laser heat input causing Ni vaporization. The rapidly vaporized metal vapor would have generated a strong stress wave, which is a hidden risk of premature failures of the welded joint [25]. A large number of fracture ridges were observed on the fracture interface (refer to Figure 12b), indicating that the fracture interface was characterized by brittle cleavage. In addition, intermetallic compounds (such as $NiTi_2$, Ni_3Ti and Ni_4Ti_3) precipitate under the action of high heat input [45–47], thus reducing tensile strength. It was interesting that both fracture mode I and mode II were brittle fractures.

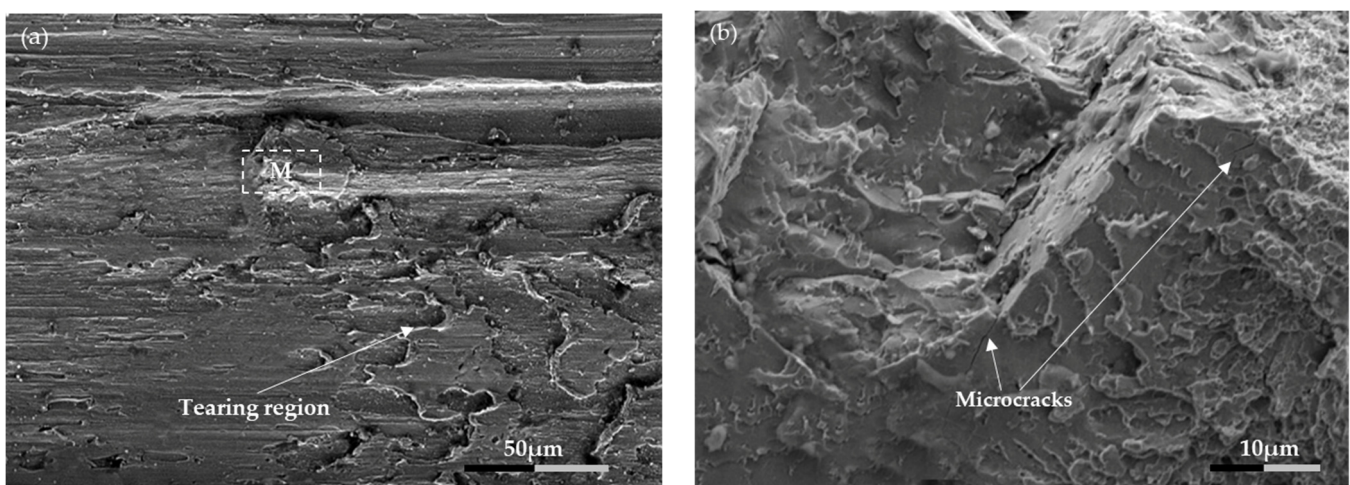


Figure 11. SEM image of fracture interface in fracture mode I: (a) Fracture surface on Ti_2AlNb side; (b) High magnification image of M.

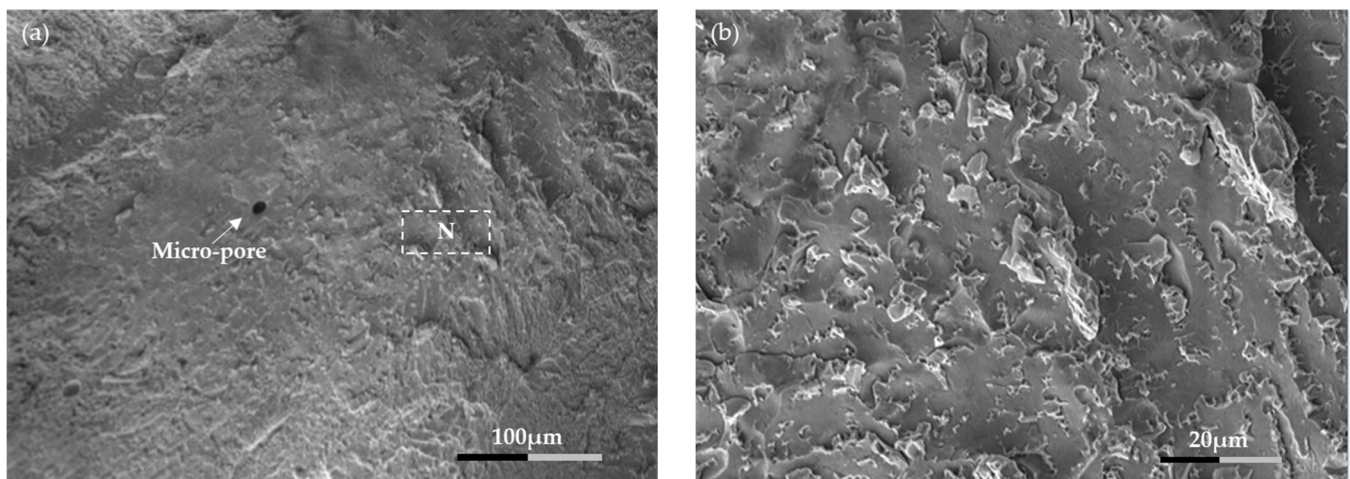


Figure 12. SEM image of fracture interface in fracture mode II: (a) Fracture surface on NiTi side; (b) High magnification image of N.

4. Conclusions

NiTi and Ti₂AlNb sheets were effectively joined by laser welding using a Nb interlayer. The following main conclusions could be drawn from the study:

(1) NiTi and Ti₂AlNb dissimilar welded joints were achieved, forming a defect-free interface with the Nb interlayer. This proves that laser welding is an effective technology that can successfully obtain NiTi to Ti₂AlNb dissimilar joints and expand their functional applications.

(2) Equiaxed grains were found in the centre of the weld, while columnar dendrites grew from the fusion line toward the centre of the weld in Figure 4. This is attributed to the gradual decrease in temperature gradient from the centre to the direction of the fusion line.

(3) The tensile strength of the lap joint was improved by optimizing the process parameters. When the laser power was 1100 W, and the welding speed was 3 mm/s, the maximum lap shear force obtained was 1236 N. It was found that the welded joint had two fracture modes. Fracture mode I showed that the tensile strength of the hypoeutectic structure formed by NiTi and Nb interlayer was stronger than the connection strength of Nb interlayer and Ti₂AlNb. Both fracture mode I and mode II had brittle-like features.

Author Contributions: Conceptualization, F.G. and Z.Z.; methodology, B.P.; software, W.K. and F.G.; validation, F.G. and Z.Z.; formal analysis, F.G.; investigation, F.G., F.B.T. and Z.Z.; resources, F.G.; data curation, F.G.; writing—original draft preparation, F.G. and F.B.T.; writing—review and editing, F.G., J.P.O. and Z.Z.; visualization, Y.L.; supervision, B.P. and Z.Z.; project administration, Z.Z. All authors have read and agreed to the published version of the manuscript.

Funding: This work was supported by National Natural Science Foundation of China (No. 51775091), Science and Technology Project of Sichuan Province (No. 2020ZDZX0015). J.P. Oliveira acknowledges Fundação para a Ciência e a Tecnologia (FCT—MCTES) for its financial support via the project UID/00667/2020 (UNIDEMI).

Institutional Review Board Statement: Not applicable.

Informed Consent Statement: Not applicable.

Data Availability Statement: Not applicable.

Acknowledgments: This work was supported by National Natural Science Foundation of China (No. 51775091), Science and Technology Project of Sichuan Province (No. 2020ZDZX0015). J.P. Oliveira acknowledges Fundação para a Ciência e a Tecnologia (FCT—MCTES) for its financial support via the project UID/00667/2020 (UNIDEMI).

Conflicts of Interest: The authors declare no conflict of interest.

References

1. Saadat, S.; Salichs, J.; Noori, M. An overview of vibration and seismic applications of NiTi shape memory alloy. *Smart Mater. Struct.* **2002**, *11*, 218–229. [[CrossRef](#)]
2. Jani, M.J.; Leary, M.; Subic, A.; Gibson, M.A. A review of shape memory alloy research, applications and opportunities. *Mater. Des.* **2014**, *56*, 1078–1113. [[CrossRef](#)]
3. Hartl, D.J.; Lagoudas, D.C. Aerospace applications of shape memory alloys. *Proc. Inst. Mech. Eng.-Part G* **2014**, *221*, 535–552. [[CrossRef](#)]
4. Appel, F.; Wagner, R. Intermetallics: Titanium Aluminides. *Encycl. Mater. Sci. Technol.* **2001**, 4246–4264.
5. Dimiduk, D.M.; Miracle, D.B.; Ward, C.H. Development of intermetallic materials for aerospace systems. *Mater. Sci. Technol.* **1992**, *8*, 367–375. [[CrossRef](#)]
6. Lutjering, G.; Williams, J.C. *Titanium*, 2nd ed.; Springer: Berlin/Heidelberg, Germany, 2007.
7. Leyens, C.; Peters, M. *Titanium and Titanium Alloys: Fundamentals and Applications*; WILEY-VCH Verlag GmbH & Co. KGaA: Weinheim, Baden-Württemberg, Germany, 2003.
8. Hagiwara, M.; Emura, S.; Araoka, A. Enhanced Mechanical Properties of Orthorhombic Ti₂AlNb-based Intermetallic Alloy. *Met. Mater. Int.* **2003**, *9*, 265–272. [[CrossRef](#)]
9. Oh, J.; Pyo, S.G.; Lee, S. Fabrication of multilayered titanium aluminide sheets by self-propagating high-temperature synthesis reaction using hot rolling and heat treatment. *J. Mater. Sci.* **2003**, *38*, 3647–3651. [[CrossRef](#)]
10. Chen, X.; Xie, F.Q.; Ma, T.J. Microstructure evolution and mechanical properties of linear friction welded Ti₂AlNb alloy. *J. Alloys Compd.* **2015**, *646*, 4–496. [[CrossRef](#)]
11. Cui, Y.; Yang, D.; Liu, B. Microstructure and mechanical properties of Ti-23Al-14Nb-3Valuminide's electron beam weld-ed joint. *Trans. China Weld. Inst.* **1998**, *19*, 130–139.
12. Chaturvedi, M.C.; Xu, Q.; Richards, N.L. Development of crack-free welds in a TiAl-based alloy. *J. Mater. Process. Technol.* **2001**, *118*, 74–78. [[CrossRef](#)]
13. Wu, Y.T.; Wei, W.S.; Koo, C.H. Diffusion bonding of Ti-25Al-10Nb alloy. *Sci. Technol. Weld. Join.* **1998**, *3*, 97–104. [[CrossRef](#)]
14. Herrmann, D.; Appel, F. Diffusion bonding of γ (TiAl) alloys: Influence of composition, microstructure, and mechanical properties. *Metall. Mater. Trans. A* **2009**, *40*, 1881–1902. [[CrossRef](#)]
15. Pan, H.; Wei, M. Key factors effecting on properties of Ti₃Al braze joints. *J. Mater. Eng.* **2009**, (Suppl. 1), 201–205.
16. Shi, M.; Xiong, J.; Zhang, G. Monitoring process stability in GTA additive manufacturing based on vision sensing of arc length. *Measurement* **2021**, *185*, 110001. [[CrossRef](#)]
17. Xue, J.L.; Peng, P.; Guo, W. HAZ Characterization and Mechanical Properties of QP980-DP980 Laser Welded Joints. *Chin. J. Mech. Eng.* **2021**, *34*, 80. [[CrossRef](#)]
18. Liu, Y.; Yao, Z.; Qin, C. Elevated temperature properties of the welding interface for Ti3Al/TC11 alloy. *Rare Met. Mater. Eng.* **2012**, *41*, 1828–1832.
19. Zeng, Z.; Cong, B.Q.; Oliveira, J.P. Wire and arc additive manufacturing of a Ni-rich NiTi shape memory alloy: Microstructure and mechanical properties. *Addit. Manuf.* **2020**, *32*, 101051. [[CrossRef](#)]
20. Oliveira, J.P.; Panton, B.; Zeng, Z. Laser joining of NiTi to Ti6Al4V using a Niobium interlayer. *Acta Mater.* **2016**, *105*, 9–15. [[CrossRef](#)]
21. Zeng, Z.; Yang, M.; Oliveira, J.P. Laser welding of NiTi shape memory alloy wires and tubes for multi-functional design applications. *Smart Mater. Struct.* **2016**, *25*, 085001. [[CrossRef](#)]
22. Sun, Z.; Ion, J. Laser welding of dissimilar metal combinations. *J. Mater. Sci.* **1995**, *30*, 4205–4214. [[CrossRef](#)]
23. Miranda, R.M.; Assuncao, E.; Silva, R.J.C. Fiber laser welding of NiTi to Ti-6Al-4V. *Int. J. Adv. Manuf. Technol.* **2015**, *81*, 1533–1538. [[CrossRef](#)]
24. Zoeram, A.S.; Mousavi, S. Laser welding of Ti-6Al-4V to Nitinol—ScienceDirect. *Mater. Des.* **2014**, *61*, 185–190. [[CrossRef](#)]
25. Song, P.; Zhu, Y.; Guo, W.; Qu, P.; Kang, H.; Wen, K. Mechanism of crack formation in the laser welded joint between NiTi shape memory alloy and TC4. *Rare Met. Mater. Eng.* **2013**, *42*, 6–9.
26. Shiue, R.H.; Wu, S.K. Infrared brazing Ti50Ni50 and Ti-6Al-4V using the BAg-8braze alloy. *Mater. Trans.* **2005**, *46*, 2057–2066. [[CrossRef](#)]
27. Zhi, Z.; Panton, B.; Oliveira, J.P. Dissimilar laser welding of NiTi shape memory alloy and copper. *Smart Mater. Struct.* **2015**, *24*, 125036.
28. Oliveira, J.P.; Fernandes, F.; Miranda, R.M. Residual stress analysis in laser welded NiTi sheets using synchrotron X-ray diffraction. *Mater. Des.* **2016**, *100*, 180–187. [[CrossRef](#)]
29. Penner, P.; Liu, L.; Gerlich, A. Dissimilar resistance spot welding of aluminum to magnesium with Zn-coated steel interlayers. *Weld. J.* **2014**, *93*, 225–231.
30. Penner, P.; Liu, L.; Gerlich, A. Feasibility study of resistance spotwelding of dissimilar Al/Mg combinations with Ni based interlayers. *Sci. Technol. Weld. Join.* **2013**, *18*, 541–550. [[CrossRef](#)]
31. Sun, M.; Niknejad, S.T.; Zhang, G. Microstructure and mechanical properties of resistance spot welded AZ31/AA5754 using a nickel interlayer. *Mater. Des.* **2015**, *87*, 905–913. [[CrossRef](#)]
32. Chen, Y.H.; Ge, J.W.; Liu, F.C. Micro laser welding of dissimilar materials between TiNi shape memory alloy and titanium alloy. *Opt. Precis. Eng.* **2014**, *22*, 2075–2080. [[CrossRef](#)]

33. Yuan, B.G.; Yu, H.P.; Li, C.F. Effect of hydrogen on fracture behavior of Ti–6Al–4V alloy by in-situ tensile test. *Int. J. Hydrogen Energy* **2010**, *35*, 1829–1838. [[CrossRef](#)]
34. Gale, W.F.; Totemeier, T.C. *Smithells Metals Reference Book*, 8th ed.; Elsevier Inc.: Amsterdam, The Netherlands, 2004.
35. Shaw, J. Simulations of localized thermo-mechanical behavior in a NiTi shape memory alloy. *Int. J. Plast.* **2000**, *16*, 541–562. [[CrossRef](#)]
36. Wu, J.; Guo, R.P.; Xu, L. Effect of Hot Isostatic Pressing Loading Route on Microstructure and Mechanical Properties of Powder Metallurgy Ti2AlNb Alloys. *J. Mater. Sci. Technol.* **2017**, *33*, 172–178. [[CrossRef](#)]
37. Otsuka, K.; Ren, X. Physical metallurgy of TiNi-based shape memory alloys. *Prog. Mater. Sci.* **2005**, *50*, 511–678. [[CrossRef](#)]
38. Servant, C.; Ansara, I. Thermodynamic assessment of the Al-Nb-Ti system. *Ber. Bunsenges. Phys. Chem.* **1998**, *102*, 1189–1205. [[CrossRef](#)]
39. Zhao, X.; Lan, L.; Sun, H. Mechanical properties of additive laser-welded NiTi alloy. *Mater. Lett.* **2010**, *64*, 628–631. [[CrossRef](#)]
40. Wu, A.; Zou, G.; Ren, J. The development status of Ti3Al alloy and its connection technology. *Aeronaut. Manuf. Technol.* **2007**, *6*, 30–35.
41. Zhao, X.; Yan, X.; Yang, Y. Wide hysteresis NiTi(Nb) shape memory alloys with low Nb content (4.5at.%). *Mater. Sci. Eng. A* **2006**, *438*, 575–578. [[CrossRef](#)]
42. Zhao, L.C.; Duerig, T.W.; Justl, S. The study of niobium-rich precipitates in a NiTiNb shape memory alloy. *Scr. Metall. Mater.* **1990**, *24*, 221–225. [[CrossRef](#)]
43. Wang, R.R.; Welsch, G.E. Joining titanium materials with tungsten inert gas welding, laser welding, and infrared brazing. *J. Prosthet. Dent.* **1995**, *74*, 521–530. [[CrossRef](#)]
44. Li, X.; Xie, J.; Zhou, Y. Effects of oxygen contamination in the argon shielding gas in laser welding of commercially pure titanium thin sheet. *J. Mater. Sci.* **2005**, *40*, 3437–3443. [[CrossRef](#)]
45. Oliveira, J.P.; Cavaleiro, A.J.; Schell, N. Effects of laser processing on the transformation characteristics of NiTi: A contribute to additive manufacturing. *Scr. Mater.* **2018**, *152*, 122–126. [[CrossRef](#)]
46. Yan, X.J.; Yang, D.Z.; Liu, X.P. Corrosion behavior of a laser-welded NiTi shape memory alloy. *Mater. Charact.* **2007**, *58*, 623–628. [[CrossRef](#)]
47. Chan, C.W.; Man, H.C. Laser welding of thin foil nickel-titanium shape memory alloy. *Opt. Lasers Eng.* **2011**, *49*, 121–126. [[CrossRef](#)]